Novel Cable-Suspended RoboCrane Support

Robert L. Williams II
Ohio University
Athens, Ohio

R.L. Williams II, 2005, "Novel Cable-Suspended RoboCrane Support", Industrial Robot: An International Journal, 32(4): 326-333.

Keywords: RoboCrane, cable-suspended robot, cable-driven, wire-actuated, self-contained base mobility.

Contact information:

Robert L. Williams II
Associate Professor
Department of Mechanical Engineering
259 Stocker Center
Ohio University
Athens, OH 45701-2979
Phone: (740) 593-1096
Fax: (740) 593-0476
E-mail:williar4@ohio.edu
URL: http://www.ent.ohiou.edu/~bobw

Novel Cable-Suspended RoboCrane Support

Robert L. Williams II
Ohio University, Athens, Ohio

Industrial Robot: An International Journal
2005

KEYWORDS

RoboCrane, cable-suspended robot, cable-driven, wire-actuated, self-contained base mobility.

ABSTRACT

The NIST RoboCrane is a cable-suspended robot with the potential to reduce the disadvantages of conventional cranes. One weakness of the RoboCrane is the need for at least three fixed rigid support points for the six overhead cable connections. In many potential applications, these rigid support points are simply not available. This article presents a new RoboCrane support concept based on rigid members, cable actuation, and cable suspension. It is self-contained and provides mobility for the required six overhead cable connections, thus extending the workspace of the existing RoboCrane. The article presents the RoboCrane support concept overview, followed by kinematics and statics analysis, plus a case study of a specific design.

Contact information:

Robert L. Williams II, Associate Professor
Department of Mechanical Engineering
259 Stocker Center, Ohio University
Athens, OH 45701-2979
Phone: (740) 593-1096
Fax: (740) 593-0476
E-mail:williar4@ohio.edu
URL: http://www.ent.ohiou.edu/~bobw

1. INTRODUCTION

Conventional cranes for construction and cargo transfer applications have the following disadvantages: non-rigid support; low payload-to-weight ratio; low resistance to wind; inaccurate control of loads; they are only used to lift and coarsely position loads; limited remote, autonomous capabilities; workers are in a hazardous area; and at any given location only one degree of freedom is controlled by the crane (i.e., the length of the lift cable between the boom and object); human workers are required with tag lines to maintain the load's remaining five degrees of freedom. This is inefficient, humans have limited strength, and it is dangerous.

To improve upon these disadvantages, the RoboCrane was developed at NIST [1-3]. The RoboCrane is an inverted Stewart Platform wherein a moving platform is controlled in six degrees of freedom via six active cables and winches. Not only can RoboCrane provide lift, but the remaining five degrees of freedom are actively controlled to be stiff and stable (over a limited range of motion and orientations). This concept was extended by NIST for a stiff, stable underwater work platform, wherein the platform may be controlled to be stationary even if surrounding seas are not [4]. The NIST RoboCrane is shown in Figure 1a; it requires three rigid overhead cable support points (not shown in Figure 1a) for hanging pairs of cables. The NIST RoboCrane has been implemented for large aircraft de-painting for the U.S. Air Force (see Figure 1b); again, three rigid overhead cable support points are required.

Figure 1a. RoboCrane at NIST

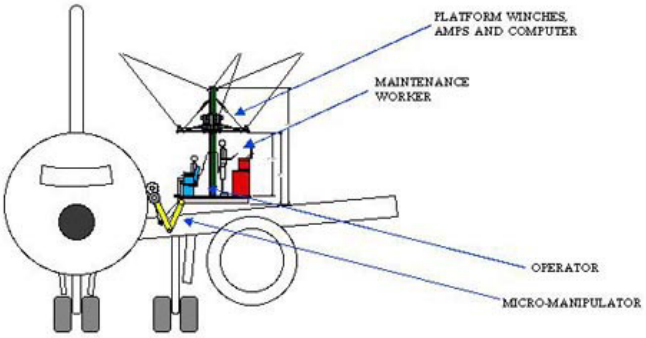

Figure 1b. RoboCrane for De-Painting

(Figures 1 are both courtesy of the NIST Intelligent Systems Division.)

Inspired by the NIST RoboCrane, many researchers have been involved with cable-suspended robots. A few of these have focused on cable-suspended crane devices. Aria et al. [5] developed a seven degree of freedom, three-cable suspended crane-type robot (the remaining freedoms are an *XY* overhead gantry, plus top and bottom turntables) for an automobile assembly line, intended for heavy products assembly. Mikulas and Yang [6] present a three-cable crane design for a lunar construction application, off-loading massive modules from a landing site, moving them, and constructing them into an operational base. Viscomi et al. [7] developed construction automation technology wherein Stewart platform cranes (i.e. RoboCranes) are central. Shanmugasundram and Moon [8] present a dynamic model of a parallel link crane with positioning and orientation capabilities, with unilateral cable constraints. Yamamoto et al. [9] propose a crane-type parallel mechanism with three active cables for handling heavy objects. Shiang et al. [10] present a parallel four-cable positioning crane for offshore loading and unloading of cargo vessels under high seas.

A primary disadvantage of the NIST RoboCrane is that six overhead rigid attachment points are required for the six active cables. In many potential applications these rigid attachment points are difficult or simply impossible to provide. Therefore, this article introduces a self-contained, deployable,

cable-suspended RoboCrane support system. Not only does it provide the required rigid cable attachment points, but it also provides mobility for these points, thus extending the workspace of the fixed-rigid-point RoboCrane. Potential applications include construction, search and rescue, and other deployable, self-contained cable-suspended robot applications. The concept was originated by Dr. James Albus of NIST and it was developed during the author's sabbatical at NIST in Gaithersburg, MD. This article presents the concept description, followed by kinematics equations and boom statics equations for control of the RoboCrane support system. We conclude with a suggested design, for which we present kinematics, workspace, and statics results.

2. ROBOCRANE SUPPORT SYSTEM DESCRIPTION

The role of the RoboCrane support system is to provide rigid, self-contained, deployable, moving overhead cable attachment points for the RoboCrane. As shown in Figure 2a, the support concept consists of rigid equilateral triangle $C_2C_3C_4$ hinged to rigid boom C_1B_0 at point C_4. Boom C_1B_0 articulates relative to the fixed standard dumpster base via a universal joint at point B_0. Boom C_1B_0 is actively controlled by cable lengths L_{B1} and L_{B2}, via motors and cable reels at points B_1 and B_2, respectively, positioning point C_1 with respect to the base. The base coordinate frame {0} is aligned as shown; its origin is placed in the center of the bottom back corner of the dumpster.

The moving, rigid RoboCrane overhead cable connection points are C_2, C_3, and C_4. As shown in Figure 2b, two active RoboCrane cables meet at each point. The RoboCrane active cable lengths are L_i, $i = 1,2,\cdots,6$. Since a good deal has been published on the RoboCrane design, kinematics, and control, [e.g. 1-4], this article focuses only on the RoboCrane support system of Figure 2a.

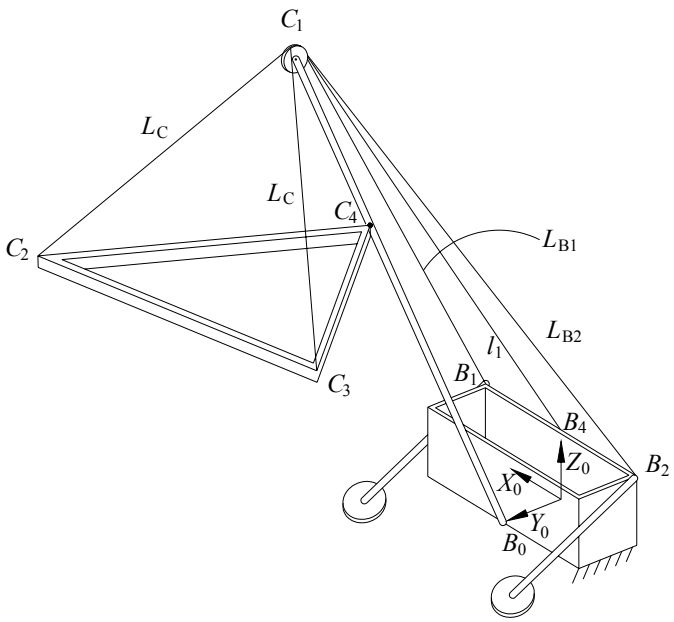

Figure 2a. RoboCrane Support Concept

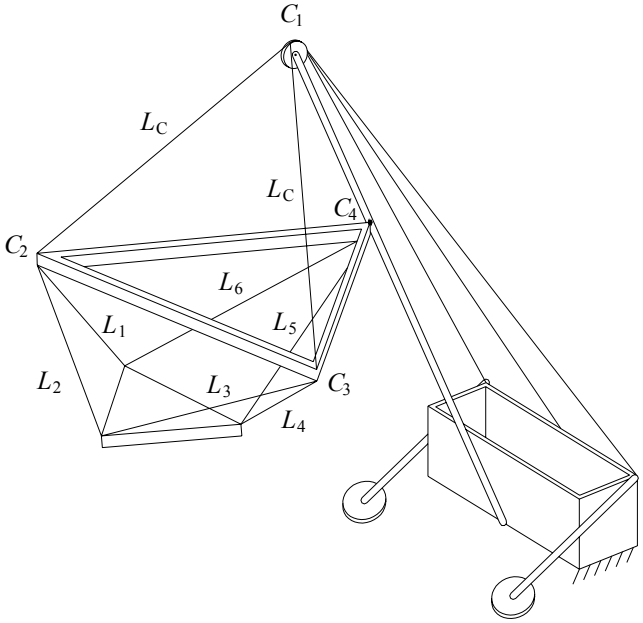

Figure 2b. Support with RoboCrane

A key aspect of this self-contained RoboCrane support system is that the configuration of the overhead equilateral triangle supporting the six RoboCrane cables is maintained by two fixed-length, passive cables. Both cables are fixed to the dumpster at point B_4, pass over pulleys at point C_1, and are fixed to moving equilateral triangle points C_2 and C_3. As cables L_{B1} and L_{B2} actively move point C_1, these passive cables move and rigidly support the equilateral triangle passively, which in turn supports the RoboCrane. At any instant during motion, the two passive cables can be seen as two lengths on either side of the pulley, L_C between point C_1 and points C_2 and C_3, and two identical lengths l_1 between moving point C_1 and fixed point B_4. With this design, having a revolute joint at C_4 (whose axis is aligned with X_0 in the nominal configuration when the boom is in the Y_0Z_0 plane), both cable portions L_C are the same length for all motion, which ensures that the Z_0 components of C_2 and C_3 are always the same (though different from the Z_0 component of C_4 in general). This passive motion control for the equilateral triangle enables a pantograph-like motion. L_C and l_1 both change during motion, but their sum is constant, set by design to keep the equilateral triangle as horizontal as possible during all motion (since the existing RoboCrane usually assumes horizontal overhead cable support points).

Thus, the RoboCrane support comprises two active degrees of freedom L_{B1} and L_{B2} plus one passive degree of freedom (which attempts to maintain horizontality for the equilateral triangle). Further, the dumpster may be deployed for additional mobility. At any dumpster location, Figures 2 show two rods with footpads to counteract the moments exerted by the weight and external loads.

We desire the equilateral triangle portion of the system to be as horizontal as possible for all motion, large workspace, and cable tensions to be as small as possible, (but they must remain in tension for all motion). These factors are competing; we present a recommended design in Section 5, including kinematics, workspace, and statics analysis results.

3. ROBOCRANE SUPPORT SYSTEM KINEMATICS

This section presents kinematics equations and solutions for the motion of the RoboCrane support system including the boom C_1B_0 and equilateral triangle $C_2C_3C_4$. The concept and kinematics equations include a passive pantograph-like near-horizontal mechanism for equilateral triangle $C_2C_3C_4$.

Kinematics relates the Cartesian position and orientation (pose) of the RoboCrane support system to the passive joint angles and active cable lengths. Figure 3 shows a kinematic diagram of the system, connected to the dumpster frame at point B_0 via a universal joint allowing boom yaw (θ_1) and pitch (θ_2). Note this reference position with the boom along the ground defines both angles θ_1 and θ_2 to be zero. The boom can be considered to be a 3R serial robot connected to the dumpster with joint angles θ_1 and θ_2, plus angle θ_3 moving the triangle with respect to the boom. Note θ_1, θ_2, and θ_3 are not controlled directly but via two active cables L_{B1} and L_{B2}, and two passive cables $L_C + l_1$. Frame $\{B_0\}$ is the same as $\{0\}$, but located at point B_0. d_1 is the length of boom C_1B_0, d_2 is the length from boom base point B_0 to the equilateral triangle hinge point C_4, and d_3 is the equilateral triangle side. Moving point C_5 is the midpoint of C_2C_3. The boom pitch angle θ_2 should be kept away from the ground position because this approaches a singularity where cables L_{B1} and L_{B2} are coplanar with the boom; in this singularity infinite force would be required to move the boom.

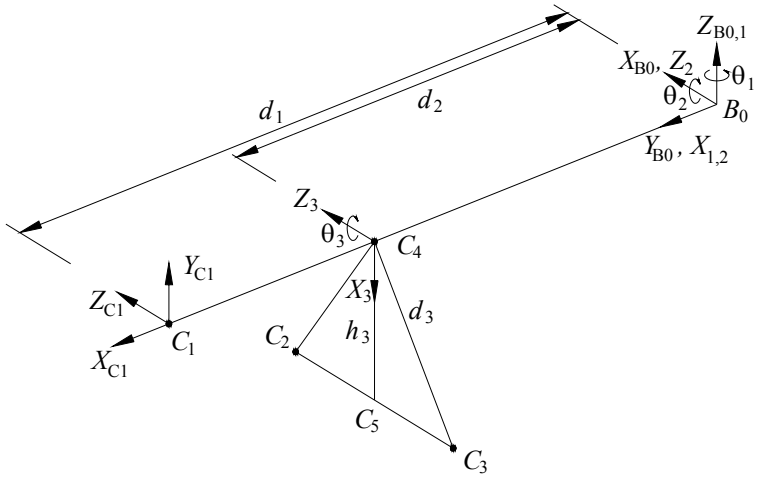

Figure 3. RoboCrane Support Kinematic Diagram

The Devavit-Hartenberg (DH) parameters [11] for this serial robot are given in Table I. Note a joint angle offset is required for i=1 since the X_0 and X_1 axes are not aligned in the zero position.

Table I. RoboCrane Support Denavit-Hartenberg Parameters

i	α_{i-1}	a_{i-1}	d_i	θ_i
1	0	0	0	$\theta_1 + 90^\circ$
2	90°	0	0	θ_2
3	0	d_2	0	θ_3

The homogeneous transformation matrices relating frames $\{C_i\}$, $i = 2,3,4,5$ (whose origins are points C_i and whose orientation is identical to that of {3}), to the world frame {0} can be found:

$$\left[{}^{0}_{C_i}\mathbf{T}\right] = \left[{}^{0}_{3}\mathbf{T}(\theta_1,\theta_2,\theta_3)\right]\left[{}^{3}_{C_i}\mathbf{T}\right] \qquad i = 2,3,4,5 \qquad \left[{}^{3}_{C_i}\mathbf{T}\right] = \begin{bmatrix} & [\mathbf{I}_3] & & \left\{{}^{3}\mathbf{C}_i\right\} \\ 0 & 0 & 0 & 1 \end{bmatrix} \tag{1}$$

The (constant) relative position vectors $\left\{{}^{3}\mathbf{C}_i\right\}$ for use in (2) are easily found by geometry. Substituting the DH parameters and $\left\{{}^{3}\mathbf{C}_i\right\}$ into (1) yields:

$$\left[{}^{0}_{C_4}\mathbf{T}\right] = \begin{bmatrix} -s_1c_{23} & s_1s_{23} & c_1 & -d_2s_1c_2 \\ c_1c_{23} & -c_1s_{23} & s_1 & d_2c_1c_2 \\ s_{23} & c_{23} & 0 & d_2s_2 \\ 0 & 0 & 0 & 1 \end{bmatrix} \tag{2}$$

where we have used the abbreviations $c_i = \cos\theta_i$ and $s_i = \sin\theta_i$, $i = 1,2$; also $c_{23} = \cos(\theta_2 + \theta_3)$ and $s_{23} = \sin(\theta_2 + \theta_3)$. The required $\left\{{}^{0}\mathbf{C}_i\right\}$ position vectors are:

$$\left\{{}^{0}\mathbf{C}_1\right\} = \begin{Bmatrix} -d_1s_1c_2 \\ d_1c_1c_2 \\ d_1s_2 \end{Bmatrix} \qquad \left\{{}^{0}\mathbf{C}_2\right\} = \begin{Bmatrix} -d_2s_1c_2 - h_3s_1c_{23} + \dfrac{d_3}{2}c_1 \\ d_2c_1c_2 + h_3c_1c_{23} + \dfrac{d_3}{2}s_1 \\ d_2s_2 + h_3s_{23} \end{Bmatrix} \quad \left\{{}^{0}\mathbf{C}_3\right\} = \begin{Bmatrix} -d_2s_1c_2 - h_3s_1c_{23} - \dfrac{d_3}{2}c_1 \\ d_2c_1c_2 + h_3c_1c_{23} - \dfrac{d_3}{2}s_1 \\ d_2s_2 + h_3s_{23} \end{Bmatrix}$$

$$\left\{{}^0\mathbf{C}_4\right\}=\begin{Bmatrix}-d_2 s_1 c_2\\ d_2 c_1 c_2\\ d_2 s_2\end{Bmatrix} \qquad \left\{{}^0\mathbf{C}_5\right\}=\begin{Bmatrix}-d_2 s_1 c_2 - h_3 s_1 c_{23}\\ d_2 c_1 c_2 + h_3 c_1 c_{23}\\ d_2 s_2 + h_3 s_{23}\end{Bmatrix} \tag{3}$$

Now, given values for θ_1, θ_2, and θ_3, it is easy to evaluate the absolute position of moving points C_i with respect to {0} using the above formulas. However, these serial angular values will not be known because it would increase cost and complexity unnecessarily to add angle sensing to the passive universal joint at B_0 and passive revolute joint at C_4. Instead, we have two choices:

1) For inverse pose kinematics (calculate the active cable lengths given the desired Cartesian pose), the upper boom point C_1 is specified at each instant (it can be moving). It is convenient to specify C_1 via angles θ_1 and θ_2 (since C_1 is constrained by the length d_1), using the first expression of (3). Then we calculate the two required cable lengths L_{B1} and L_{B2}:

$$L_{B1}=\left\|{}^0\mathbf{C}_1-{}^0\mathbf{B}_1\right\| \qquad L_{B2}=\left\|{}^0\mathbf{C}_1-{}^0\mathbf{B}_2\right\| \tag{4}$$

The passive revolute angle θ_3 will be determined after the forward pose kinematics case below since it is the same for both options.

2) For forward pose kinematics (calculate the Cartesian pose given the active cable lengths), the two cable lengths L_{B1} and L_{B2} are known from their winch angular feedback measurements. Upper boom point C_1 is calculated given these two cable lengths. From Figure 2a, point C_1 is the intersection of three spheres: fixed boom radius d_1 centered at B_0, radius L_{B1} centered at B_1, and radius L_{B2} centered at B_2. The intersection of three spheres is the basis for the forward pose kinematics solutions of various NIST-developed cable devices; this solution may be found in [12]. Point C_1 is found using that method:

${}^0\mathbf{C}_1$ is found from the intersection of three spheres: $({}^0\mathbf{B}_1, L_{B1})$, $({}^0\mathbf{B}_2, L_{B2})$, and $({}^0\mathbf{B}_0, d_1)$.

Note the ordering of the three spheres is very important to avoid algorithmic singularities [12]. The above ordering is the only successful possibility since points B_1 and B_2 always have the same Z_0

coordinate. Given ${}^0\mathbf{C}_1$ we can calculate passive universal joint angles θ_1 and θ_2 from an inverse position kinematics solution of the expression for $\left\{{}^0\mathbf{C}_1\right\} = \left\{P_x \quad P_y \quad P_z\right\}^T$ in (3):

$$\theta_1 = \tan^{-1}\left(\frac{-P_x}{P_y}\right) \qquad\qquad \theta_2 = \sin^{-1}\left(\frac{P_z}{d_1}\right) \tag{5}$$

Now we can determine θ_3; it is done in the same manner for both of the above cases. Figure 4a shows a side view of the system concept. This side view shows a planar representation of the passive equilateral triangle pantograph cables; $l_1 = \|C_1B_4\|$ are the real variable portions of the two passive pantograph cables, and $l_2 = \|C_1C_5\|$ is a virtual variable cable representing the planar projections of the cables' portions L_C (see Figure 2a and visualize the plane $C_1C_2C_3$; l_2 bisects this triangle).

$$l_2 = \sqrt{L_C^2 - d_3^2/4} \qquad\qquad \theta_3 = -\cos^{-1}\left[\frac{h_3^2 + (d_1 - d_2)^2 - l_2^2}{2h_3(d_1 - d_2)}\right] \tag{6}$$

θ_3 is negative in (6) due to its definition in Figures 3 and 4a. This pantograph mechanism will be designed to attempt to maintain the equilateral triangle as near horizontal as possible for all motion. It can be exact only at one θ_2 angle. If the triangle is perfectly horizontal, $\theta_3 = -\theta_2$.

We need the (actual) cable lengths L_C for θ_3 determination. The two passive pantograph cables (running from B_4, over pulleys at C_1, connecting to points C_2 and C_3) are of fixed length $L_{nom} = l_1 + L_C$. Therefore, $L_C = L_{nom} - l_1$. Let us fix L_{nom} by design, requiring the equilateral triangle to be exactly horizontal ($\theta_3 = -\theta_2$) at a nominal value of the boom pitch angle (θ_{2nom}) and for the central value of the yaw angle, $\theta_{1nom} = 0$; θ_{2nom} should be in the middle of the allowable θ_2 range, or some other nominal, often-used configuration. At the nominal configuration we have $L_{nom} = l_{1nom} + L_{Cnom}$, where $l_{1nom} = \|C_{1nom}B_4\|$. From (6), we have $L_{Cnom} = \sqrt{l_{2nom}^2 + d_3^2/4}$; the nominal virtual pantograph cable

length is $l_{2nom} = \|C_{1nom}C_{5nom}\|$. The nominal locations of C_1 and C_5 are found by substituting $\theta_1 = 0$ and $\theta_2 = \theta_{2nom}$ into the first and last expressions of (3). Finally, given θ_1, θ_2, and θ_3 from (5) and (6) we can calculate the position vectors for all moving points C_i from (3), for general configurations. This approach was implemented in Matlab to demonstrate the near-horizontal pantograph-like mechanism in a Y_0Z_0 planar projection of the 3D system (see Figure 4b).

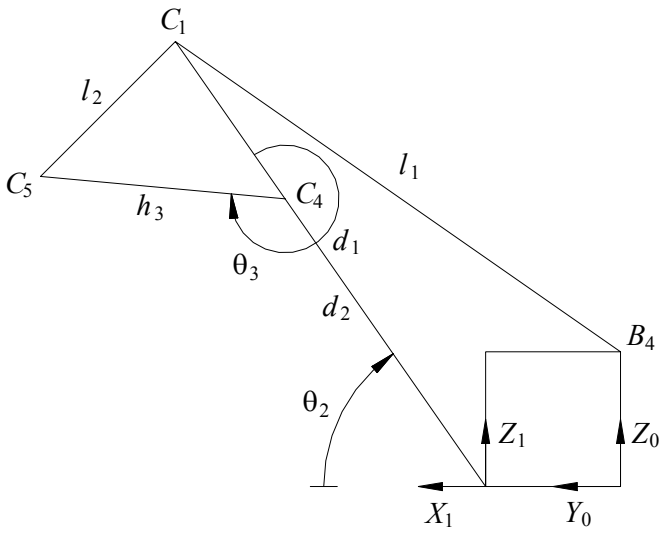

Figure 4a. Side View

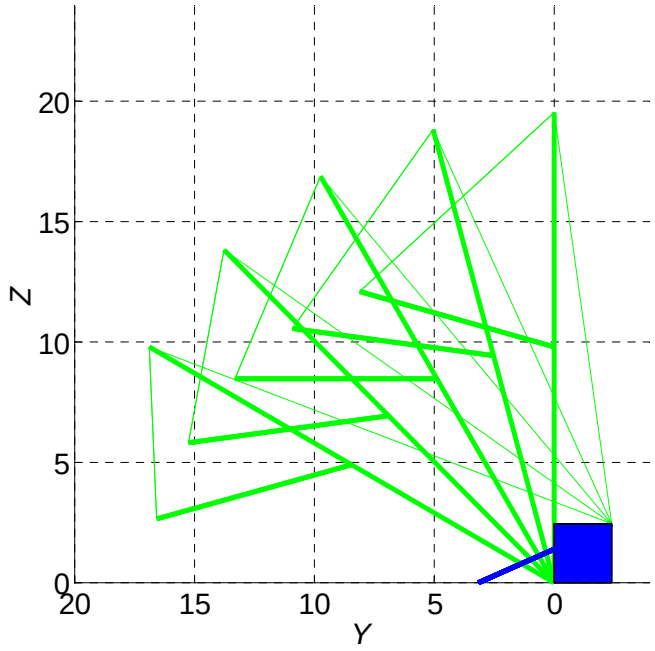

Figure 4b. Horizontal Mechanism Demonstration

4. ROBOCRANE SUPPORT SYSTEM BOOM STATICS

A standard 3D statics model has been derived and implemented for the RoboCrane support system. The details are not given in this article, but are available from the author. This section highlights a potential problem of slack cables during boom control. This will never be a problem for the passive pantograph-like cable tensions since the horizontality pantograph mechanism design guarantees positive tension for both sides (on either side of the pulleys at point C_1, in the absence of extreme downward dynamic motions) of the passive cables, since the loads at C_2 and C_3 will maintain tension via gravity at all times. However, negative cable tension is a potential problem for the active boom-guiding cables with lengths L_{B1} and L_{B2}.

As seen in Figure 2a, boom-moving cables L_{B1} and L_{B2} are actively controlled to indirectly control the yaw angle θ_1 and pitch angle θ_2 (see Figure 3). These cables can lift the boom from horizontal to vertical ($\theta_{2ABS} = 0 \rightarrow 90^\circ$), although the extremes should be avoided due to near-singularity conditions, leading to higher tensions near the ground and near vertical. The problem we now present is with the yaw angle θ_1; if this angle is commanded to a value that is too large, one of the boom-moving cables will require impossible pushing forces to maintain static equilibrium. Figure 5 shows the top view of these boom-moving cables. When the X_0Y_0 projection of boom B_0C_1 becomes collinear with the X_0Y_0 projection of cable L_{B1}, we have reached the positive limit on θ_1 (by symmetry, the equal, negative limit on θ_1 occurs when B_0C_1 becomes collinear with L_{B2}).

The value of the limiting θ_1 angles, $\pm\theta_{1LIMIT}$, is dependent on the locations of B_1 and B_2, plus dumpster dimensions d_{B1} and d_{B2}. θ_{1LIMIT} is not dependent on boom length d_1 or boom pitch angle θ_2 (from (5) θ_1 is independent of vertical components). From the collinear projection constraints and Figure 5, we can calculate $\pm\theta_{1LIMIT}$:

$$\pm\theta_{1LIMIT} = \pm\tan^{-1}\left[\frac{d_{B1}/2}{d_{B2}(1-f_2)}\right] \tag{14}$$

From Figure 5 we see that the largest θ_{1LIMIT} will result from moving points B_1 and B_2 as far forward in the dumpster Y_0 direction as possible. f_2 is the fraction of d_{B2} along the Y_0 direction where points B_1 and B_2 are placed (the $f_2 = 0$ case is shown in Figure 5; $f_2 = 1$ corresponds to B_1 and B_2 placed at the forward edge of the dumpster). Figure 6 shows θ_{1LIMIT} for f_2 fractions from 0 to 1, for a standard-sized (see Section 5) dumpster.

We see that $\pm\theta_{1LIMIT}$ increases with increasing f_2, as predicted from the geometry of Figure 5. Figure 6 verifies that for large limits on θ_1 we must move the points B_1 and B_2 as far forward as possible ($f_2 = 1$). If $f_2 = 1$, the theoretical limit on θ_1 is $\pm 90^\circ$, allowing for a large range of motion. All motion should be kept well away from the specific $\pm\theta_{1LIMIT}$ for any given design, to safely avoid the slack cable problem and the resulting catastrophic loss of control. However, $f_2 = 1$ also corresponds to a significant increase in statics cable tensions due to approaching statics singularities and a loss of half the moment arm for lifting the boom (compared to $f_2 = 0$); therefore in this article, we choose $f_2 = 0$, placing points B_1 and B_2 on the dumpster back top surface (as seen in Figure 5), yielding $\pm\theta_{1LIMIT} = \pm 51.3^\circ$. A compromise is possible, say choosing $f_2 = 0.5$ for $\pm\theta_{1LIMIT} = \pm 68.2^\circ$, balancing a larger workspace with worse kinematic horizontality and worse statics tensions.

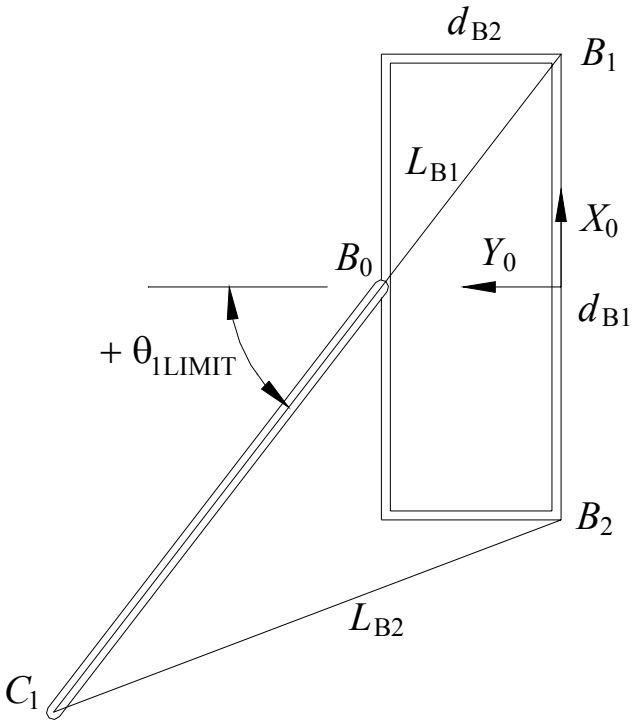

Figure 5. θ_{1LIMIT} **Determination**

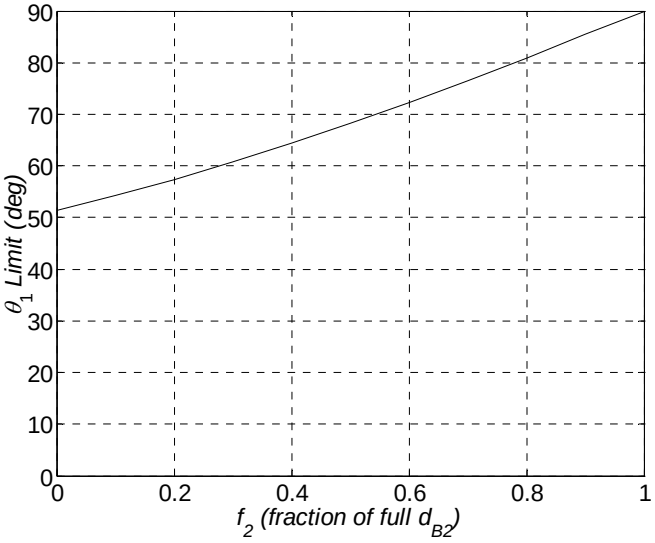

Figure 6. θ_{1LIMIT} **, Varying** B_1 **and** B_2 **Locations**

5. OVERALL ROBOCRANE SUPPORT SYSTEM DESIGN

This section presents a recommended good overall RoboCrane support system design considering the competing kinematic horizontality, workspace, and statics issues (more details are available from [13]). For analysis and design purposes, we have adopted the following parameters in this article (in SI units).

$d_{B1} = 6.096$	Dumpster length (20')
$d_{B2} = 2.438$	Dumpster width (8')
$d_{B3} = 2.438$	Dumpster height (8')
$d_M = 7.620$	Length of moment resisting rods (25')
$f_2 = 0$	Fraction of d_{B2} along Y_0 for mounting B_1 and B_2
$d_1 = 18.288$	Boom length C_1B_0 (60')
d_2 (design variable)	C_4B_0 length along boom to equilateral triangle connection
d_3 (design variable)	Equilateral triangle side $C_2C_3 = C_3C_4 = C_4C_2$
B_{4y} (design variable)	Base mounting location along Y_0 for pantograph cables

Design tradeoffs were studied, particularly between good horizontality and large workspace area. Good horizontality always means that the equilateral triangle will be small, not even extending the working range to point C_1, let alone beyond it as desired. Good horizontality designs can also exist near designs where the desired motion ranges are partially reduced due to imaginary kinematics solutions. Good X_0Y_0 workspace area designs mean large triangles (with not the best horizontality), mounted low on the spar (with poor associated Z_0 heights). There is also a tradeoff considering only workspace, between high X_0Y_0 workspace area and acceptable Z_0 height characteristics: large X_0Y_0 areas can have poor height characteristics, even dipping the triangle into the ground! Good designs for Z_0 height characteristics (proper vertical clearance, minimum variation in Z_0 over all motion) can be associated with poor X_0Y_0 areas. Statics had the least effect in choosing good designs; the important cable tension magnitudes were fairly steady over a wide range of varying parameters. However, statics was in one

sense the most important analysis because it pointed out that some designs must be avoided because they require negative cable tensions during part of the range of motion.

We did not attempt global optimal design of the system subject to horizontality, workspace, and statics issues; rather, in this section we propose a good, acceptable design for a practical machine. This applies to a desired range of motion: $\theta_1 = \left[-45^\circ, 45^\circ\right]$ and $\theta_2 = \left[30^\circ, 90^\circ\right]$. A good design considering horizontality, workspace, and statics is:

$$d_2 = \tfrac{1}{2}(d_1),\ d_3 = d_1 - d_2, \text{ and } B_{4y} = 0$$

Figures 7 show the kinematic horizontality results (7a absolute and 7b relative); Figures 8 show the X_0Y_0 workspace projection (8a) and associated workspace Z_0 heights (8b); and Figure 9 shows the statics results for this 'good design', for all motion $\theta_1 = \left[-45^\circ, 45^\circ\right]$ and $\theta_2 = \left[30^\circ, 90^\circ\right]$.

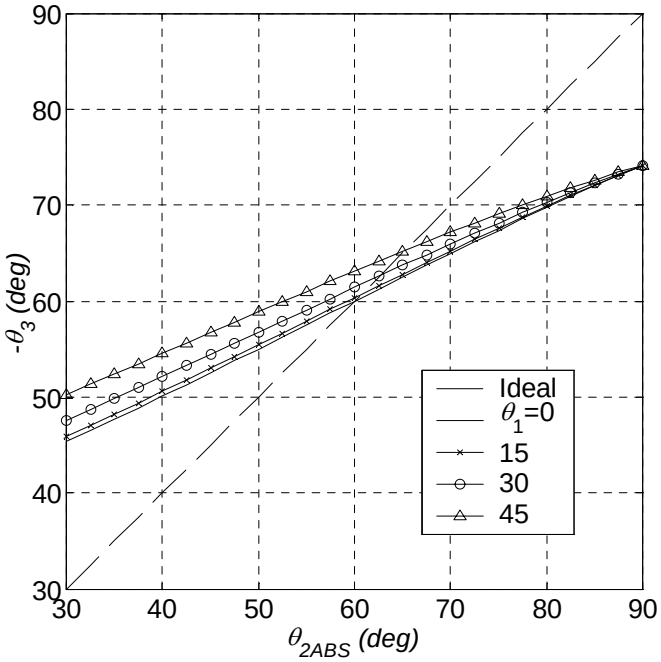

Figure 7a. Angle θ_3

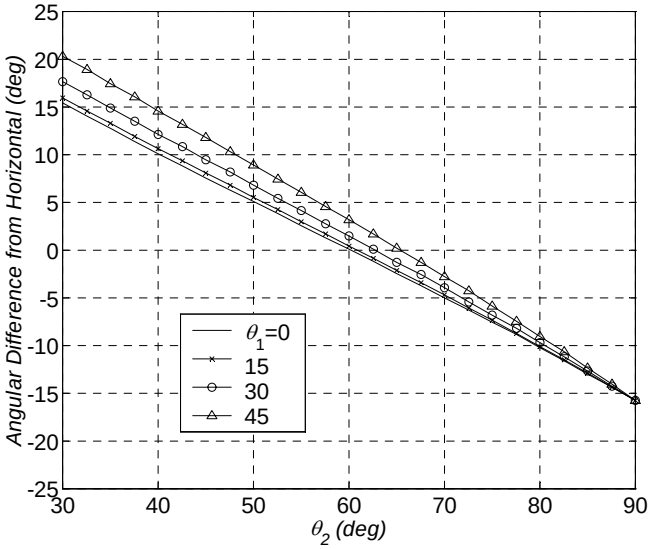

Figure 7b. Horizontality Deviation

Figures 7a and 7b show that the horizontality associated with our chosen design is not very good at the θ_2 extremes; motions near $\theta_{2nom} = 60^\circ$ maintain horizontality much better. The dashed line in

Figure 7a is the desired perfect absolute horizontality, and ideal relative values for Figure 7b are zero. Note that perfect horizontality is only possible at one location, at the nominal $\theta_{2nom} = 60^\circ$, with $\theta_1 = 0$. This design has a relatively large X_0Y_0 workspace area as shown in Figure 8a. The associated Z_0 heights shown in Figure 8b are acceptable (at least they are above the ground for all motion; they dip into the ground for some designs); however, the Z_0 variation is rather large, another cost of large X_0Y_0 workspace area (reduced horizontality is also associated with large X_0Y_0 workspace area). The statics results in Figure 9, showing active tension t_{B1} and passive tension t_C, are typical of a wide range of possible designs; statics does not make much difference in design. Active tension t_{B2} is always less than t_{B1} for $0 < \theta_1 \le 45^\circ$; due to symmetry they swap roles for $-45^\circ < \theta_1 \le 0$, so Figure 9 covers the highest tensions for all motion. In this article, we assume that identical 1000 N weights act vertically down at each of the four points $\{C_i\}$, $i = 1, 2, 3, 4$ (one on the boom tip to include a possible lifting cable there, the other three on the equilateral triangle vertices to provide a simple model for RoboCrane cable tensions). The chosen design does not require any negative cable tensions for the entire design range of motion.

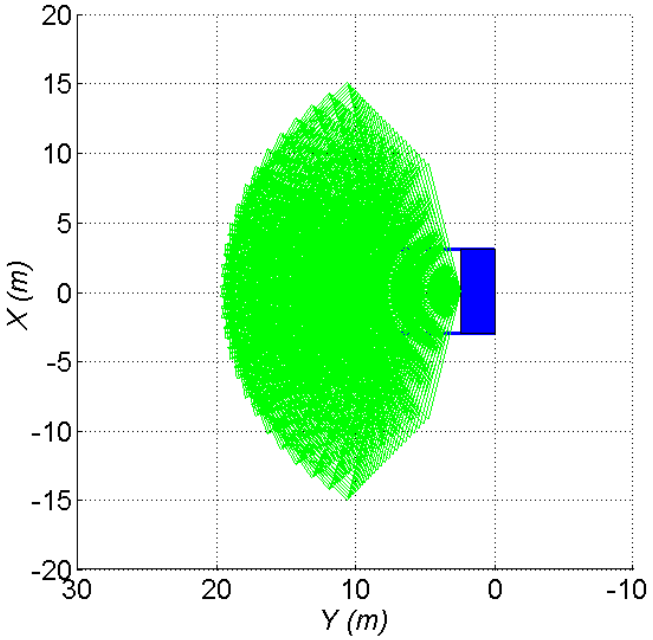

Figure 8a. Workspace Projection

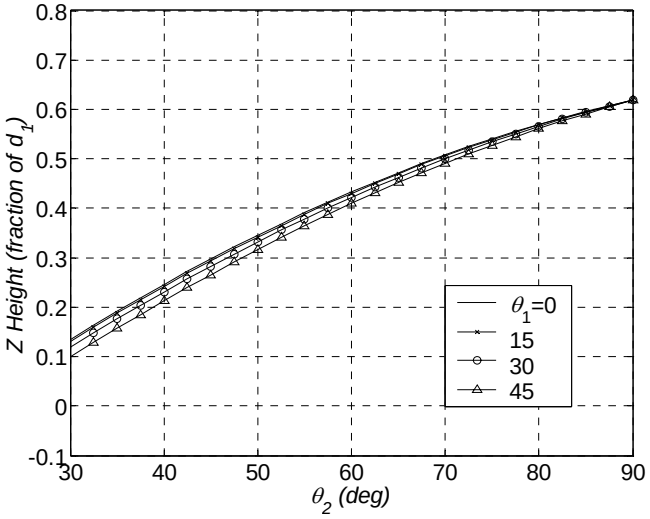

Figure 8b. Associated Z_0 Heights

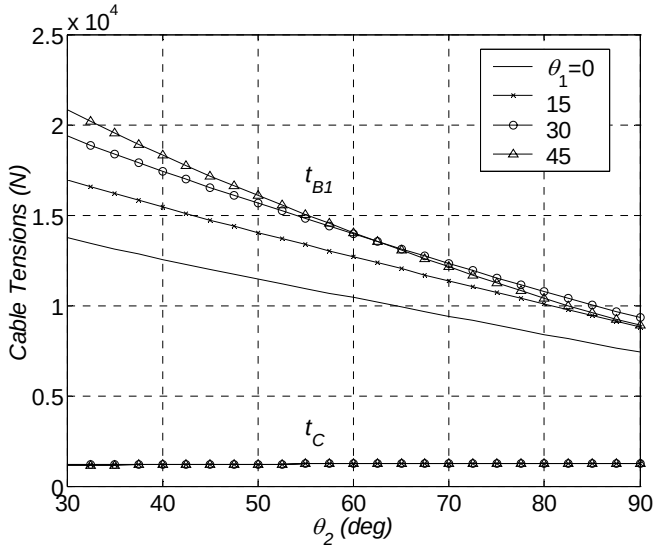

Figure 9. Statics Results

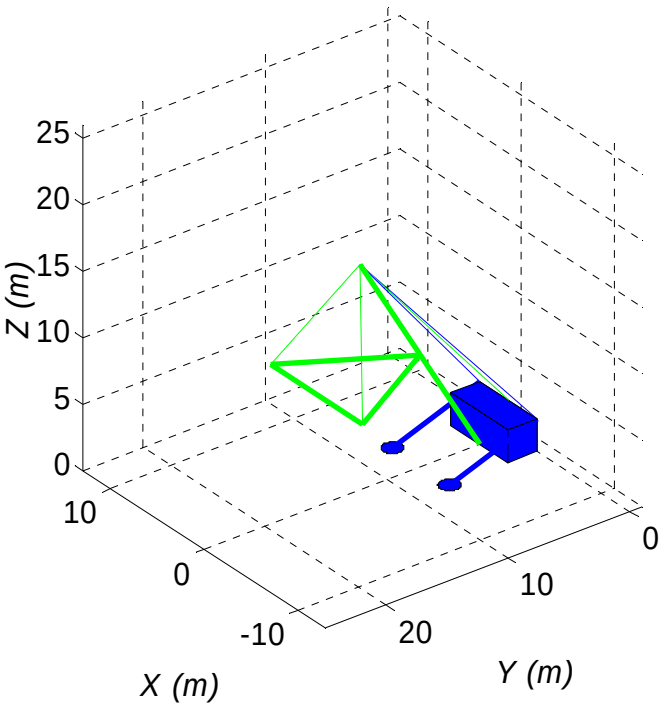

Figure 10. Example Design

Figure 10 shows a 3D Matlab rendition of the chosen design, in the motion configuration $\theta_1 = 0$ and $\theta_2 = \theta_{2nom} = 60^\circ$. Again, the design of Figure 10 is not a global optimum, but a good practical design based on tradeoffs and practical considerations. The mathematical tools in this article can be used to check design candidates for specific automated construction applications.

6. CONCLUSION

This article has introduced a new RoboCrane support system based on a combination of rigid members and cable-suspended technology, for extending the potential of RoboCrane in various applications. The support system itself has a total of three degrees of freedom: the boom is driven by two active cables, and a rigid equilateral triangle hinged to the boom is kept nearly horizontal via pantograph-like cables, representing a passive degree of freedom. The role of the equilateral triangle is

to provide a rigid, self-contained, mobile overhead support for the six active RoboCrane cable attachment points.

Presented were kinematics, workspace, and statics analyses for the proposed system, including a specific recommended design. These analyses also form the basis for control equations. Forward and inverse kinematics solutions were presented, plus analysis of the horizontality of the passive pantograph-like cable mechanism (since the conventional RoboCrane assumes horizontal overhead cable connection points). Workspace was determined, both planar projection workspace and the associated vertical heights. Statics analyses involved calculating active and passive cable tensions, plus internal joint forces. Tradeoffs were found amongst the various analyses; for example, a design for good equilateral triangle horizontality leads to a poor workspace, and vice versa. Statics was not a major factor in choosing good designs, except for one all-important characteristic: statics analysis exposed conditions when impossible, negative cable tensions are required for certain motions and configurations. These must be avoided completely by design, to avoid catastrophic loss of control. Also, statics will be very important in designing the system to resist all loads, especially at the pivot point C_4. This RoboCrane support system concept shows promise as a self-contained, mobile, rigid support system for a variety of deployable cable-suspended robot applications where rigid supports are not available.

ACKNOWLEDGEMENTS

The author gratefully acknowledges support for this work from the NIST Intelligent Systems Division, via Grant #70NANB2H0130. The novel RoboCrane support system concept originated with Dr. James S. Albus, Senior NIST Fellow, and design suggestions were contributed by Roger V. Bostelman of NIST.

REFERENCES

[1] James S. Albus, 1989, "Cable Arrangement and Lifting Platform for Stabilized Load Lifting", U.S. Patent 4,883,184, November 28, 1989.

[2] N.G. Dagalakis, J.S. Albus, B.-L. Wang, J. Unger, and J.D. Lee, 1989, "Stiffness Study of a Parallel Link Robot Crane for Shipbuilding Applications", Journal of Offshore Mechanical and Architectural Engineering, 111(3): 183-193.

[3] J.S. Albus, R. Bostelman, and N.G. Dagalakis, 1993, "The NIST ROBOCRANE", Journal of Robotic Systems, 10(5): 709-724.

[4] R.V. Bostelman, J.S. Albus, and A.M. Watt, 1996, "Underwater Work Platform Support System", U.S. Patent 5,507,596, April 16, 1996.

[5] T. Aria, H. Osumi, and H. Yamaguchi, 1990, "Assembly Robot Suspended by Three Wires with Seven Degrees of Freedom", MS90-807, 11th International Conference on Assembly Automation, SME, Dearborn, MI.

[6] M.M. Mikulas Jr. and L.-F. Yang, 1991, "Conceptual Design of a Multiple Cable Crane for Planetary Surface Operations", NASA Technical Memorandum 104041, NASA LaRC, Hampton, VA.

[7] B.V. Viscomi, W.D. Michalerya, and L.-W. Lu, 1994, "Automated Construction in the ATLSS Integrated Building Systems", Automation in Construction, 3(1): 35-43.

[8] A.P. Shanmugasundram and F.C. Moon, 1995, "Development of a Parallel Link Crane: Modeling and Control of a System with Unilateral Cable Constraints", ASME International Mechanical Engineering Congress and Exposition, San Francisco CA, DSC 57-1: 55-65.

[9] M. Yamamoto, N. Yanai, and A. Mohri, 1999, "Inverse Dynamics and Control of Crane-Type Manipulator", IEEE/RSJ International Conference on Intelligent Robots and Systems, 2: 1228-1233.

[10] W.-J. Shiang, D. Cannon, and J. Gorman, 1999, "Dynamic Analysis of the Cable Array Robotic Crane", IEEE International Conference on Robotics and Automation, Detroit MI, 4: 2495-2500.

[11] J.J. Craig, 1989, Introduction to Robotics: Mechanics and Control, Addison Wesley Publishing Co., Reading, MA.

[12] R.L. Williams II, J.S. Albus, and R.V. Bostelman, 2004, "3D Cable-Based Cartesian Metrology System", Journal of Robotic Systems, 21(5): 237-257.

[13] R.L. Williams II, 2003, "NIST Sabbatical Report: 2. Self-Contained Automated Construction Crane System", submitted to Dr. James S. Albus, NIST Fellow, NIST Grant #70NANB2H0130, May 31.